Table 4 Capture orbit initiation for day 1 of launch window (full- and half-system scenarios)

	Desired orbit						Achieved orbit		
Mode	Periapsis radius (km)	Semimajor axis (km)	Impulsive velocity requirement (m/s)	Approach periapsis (km)	Burn initiation point θ_s (deg)	Burn time (min)	Periapsis radius (km)	Semimajor axis (km)	Actual velocity increment (m/s)
Full system[a]	4100	20,000	985	4160	40	14	4100	20,000	1000
Half system[b]	4100	20,000	985	4160	40	25 3[c]	4105 4100[c]	40,000 20,000[c]	900 100[c]

[a]Full system uses all four thrusters. [b]Half system uses two of the four thrusters. Capture executed in two burns. [c]Second burn.

tion, if the burn initiation point were to be the same as for the full system (θ_s is 20 deg in Fig. 3) and the same steering law were to be utilized (thrust in the negative velocity direction), the periapsis radius would become smaller than the radius of Mars before the spacecraft velocity could be sufficiently reduced to capture the spacecraft around Mars. Therefore, for backup half-system operation, the required burn initiation position is 40 deg before the periapsis (θ_s is 40 deg in Fig. 4).

Because the requirement for half-system operation can be determined only after initiation of the burn, the burn initiation point for the full system is also retracted to 40 deg before periapsis to assure viable half-system capability. The full-system burn will thus no longer be centered around the periapsis; this imposes an additional 5 m/s in finite-burn penalty and reduces the periapsis radius by an additional 10 km. This requires a target periapsis radius of 4160 km at TCM 4 to obtain the desired 4100 km at the end of the insertion burn. Table 4 shows the capture scenario for a redundant system (for full- or half-system operation).

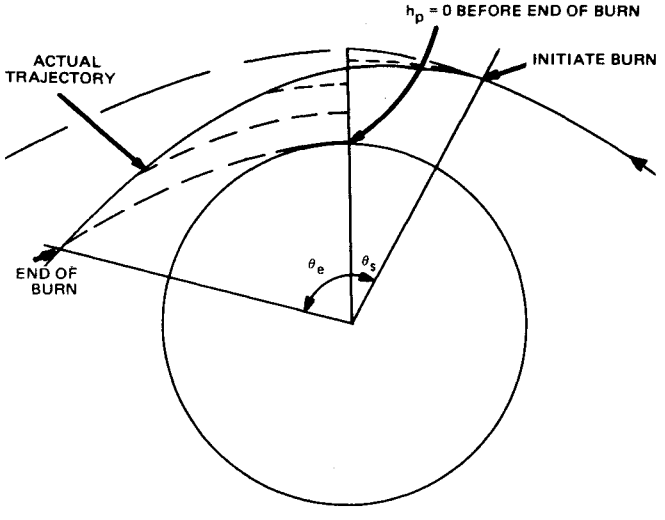

Fig. 3 Capture using two thrusters and $\theta_s = 20$ deg.

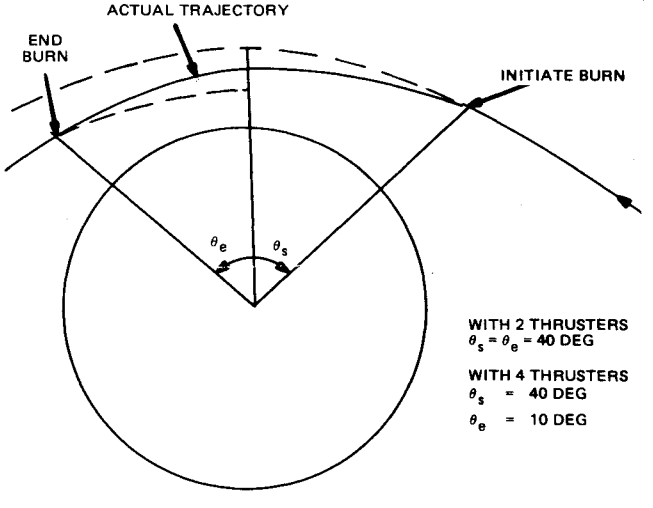

Fig. 4 Capture using two or four thrusters and $\theta_s = 40$ deg.

Conclusion

This paper has discussed the implication of a low-thrust insertion into a Mars orbit using four 110-lbf thrusters. The strategy includes insertion into an elliptical capture (drift) orbit (4100 × 20,000 km), targeting for a 4150-km periapsis to compensate for reduction in periapsis altitude during burn, initiating the burn at about 20 deg before the periapsis (40 deg if half-system capability is desired), and minimizing the finite-burn penalty by pitching the spacecraft during the burn to align the thrust vector parallel to the negative velocity vector.

Reference

[1]"Mars Observer Trajectory Characteristics," Enclosure 3 to RFP JM-2-5607-481, NASA JPL, Jan. 31, 1985.

Tethered Subsatellite Swinging from Atmospheric Gradients

Junjiro Onoda* and Naoyuki Watanabe†
The Institute of Space and Astronautical Science, Tokyo, Japan

Nomenclature

C_D = aerodynamic drag coefficient
D = aerodynamic drag force
EA = longitudinal rigidity of tether
l = tether length
l_o = tether length in zero-tension state
m = mass of subsatellite
R = radius of orbit of main satellite
S = equivalent drag area (involving both subsatellite and tether)
T = tether tension

Received March 27, 1987; revision received June 4, 1987.

*Associate Professor, Research Division of Space Transportation. Member AIAA.
†Research Associate, Research Division of Space Transportation.

X,Z = location of subsatellite in orbit-fixed coordinates
x,z = infinitesimal displacement of subsatellite from steady-state equilibrium point, see Eq. (17)
ϵ = see Eq. (22)
θ = angle between local vertical and tether line, see Fig. 1
λ = see Eq. (18)
ρ = density of atmosphere
Ω = rotational angular rate of Earth
ω = orbital angular rate

Subscript

s = steady-state solution

Introduction

A TETHERED subsatellite deployed in a low-altitude orbit has been proposed as a means of upper-atmospheric experiments. Many works on the dynamics and control of the tethered satellite systems, especially in the deployment/retrieval process, have been reported. Concerning the vibrational motion around a steady-state equilibrium point of tethered satellite in a circular orbit, the effect of the atmosphere seems to have been regarded to increase the stability. However, Bainum et al.[1] recently showed that atmospheric effects can increase the instability of out-of-(orbit)-plane motion of a subsatellite caused by a parametric excitation. In addition, Yuhara et al.[2] showed a numerical example of unstable in-plane swinging motion of an uncontrolled tethered subsatellite deployed in low-altitude orbit. Yuhara et al. have suggested only that it is due to the atmosphere, and the mechanism of the instability, i.e., what causes the instability, was not shown. In this Note, it is clearly shown for the first time that, based on a simple model, the instability is caused by the atmospheric density gradient.

Equations of Motion

Since the purpose of this Note is to clarify the mechanism of the instability, the mathematical model is simplified as much as possible by making the following assumptions.

1) The mass and the bending rigidity of the tether are negligible.

2) The mass of the subsatellite is very small compared with the main satellite. Hence, the center of mass of the total system can be regarded as the main satellite.

3) The total system is moving in a circular orbit around the spherical Earth. The inclination of the orbit is zero.

4) The atmosphere rotates with the Earth.

5) The density of the atmosphere is a function of altitude only.

6) Both main and subsatellites can be regarded as mass points.

7) Aerodynamic drag force is proportional to the atmospheric density and square of velocity.

8) Most of the effective aerodynamic drag on the tether acts on the lowest small portion of the tether, and it can be approximated by a drag force on the subsatellite.

The equations of motion of the subsatellite then can be written as follows in the orbit-fixed coordinates centered at the main satellite with the X axis along the local vertical and the Z axis in the orbital plane, as shown in Fig. 1.

$$m(\ddot{X} - 2\omega\dot{Z} - 3\omega^2 X) = -T\cos\theta - D\dot{X}/v \tag{1}$$

$$m(\ddot{Z} + 2\omega\dot{X}) = -T\sin\theta - D \tag{2}$$

$$T = EA(l - l_0)/l_0 \tag{3}$$

$$l^2 = X^2 + Z^2 \tag{4}$$

$$\cos\theta = X/l, \qquad \sin\theta = Z/l \tag{5}$$

$$D = \tfrac{1}{2}\rho C_D S v^2 \tag{6}$$

$$v^2 = \{(\omega - \Omega)R + \dot{Z}\}^2 + \dot{X}^2 \tag{7}$$

$$\rho = \text{a function of } R + X \tag{8}$$

where

$$|X/R| \ll 1, \qquad |Z/R| \ll 1 \tag{9}$$

have been assumed and they have been neglected compared with unity.

Linearization of Equations of Motion

It is clear that steady-state solutions of Eqs. (1–8), i.e., X_s, Z_s, T_s, ρ_s, l_s, satisfy the following equations.

$$3m\omega^2 X_s - T_s X_s/l_s = 0 \tag{10}$$

$$T_s Z_s/l_s + \tfrac{1}{2}\rho_s C_D S\omega^2 R^2(1 - \Omega/\omega)^2 = 0 \tag{11}$$

$$T_s = EA(l_s - l_0)/l_0 \tag{12}$$

$$l_s^2 = X_s^2 + Z_s^2 \tag{13}$$

$$\rho_s = \text{a function of } X_s \tag{14}$$

Therefore, by using these equations, the equations of infinitesimal additional motion, x,y, around the preceding steady-state solution, can be written as follows:

$$\ddot{x} - \frac{3Z_s}{R(1-\Omega/\omega)}\omega\dot{x} - 2\omega\dot{z} + \frac{3l_0\omega^2 X_s^2}{l_s^2(l_s - l_0)}x + \frac{3l_0\omega^2 X_s Z_s}{l_s^2(l_s - l_0)}z = 0 \tag{15}$$

$$\ddot{z} + 2\omega\dot{x} - \frac{6Z_s}{R(1-\Omega/\omega)}\omega\dot{z} + 3\omega^2 Z_s\left[\frac{X_s l_0}{l_s^2(l_s - l_0)} + \lambda\right]x + 3\omega^2\frac{l_s^3 - l_0 X_s^2}{l_s^2(l_s - l_0)}z = 0 \tag{16}$$

where

$$x = X - X_s, \qquad z = Z - Z_s \tag{17}$$

and

$$\rho = \rho_0 \exp(-\lambda X) \tag{18}$$

has been assumed.

Stability Investigation

For a subsatellite deployed to a low-altitude orbit, as shown in Fig. 1, it is obvious that

$$X_s < 0, \qquad Z_s < 0, \qquad l_s > l_0 \tag{19}$$

Because usually

$$\lambda > 2/R \tag{20}$$

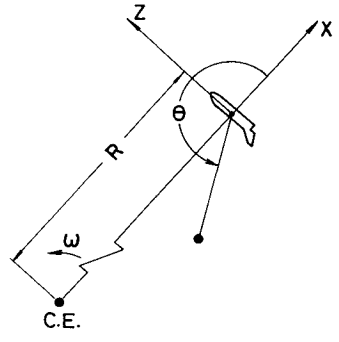

Fig. 1 Tethered satellite system.

Table 1 Examples of eigenvalues and eigenvectors

$\rho_s C_D S/m$, m^{-1}, $\times 10^{-9}$	λ, m^{-1}, $\times 10^{-4}$	Eigenvalues, s^{-1}	Eigenvectors x	Eigenvectors z
2	1.5	$-5.25 \times 10^{-5} \pm 1.42 \times 10^{-2} i$	$9.82 \times 10^{-1} \pm 0i$	$8.37 \times 10^{-2} \pm 1.69 \times 10^{-1} i$
		$4.15 \times 10^{-5} \pm 2.23 \times 10^{-3} i$	$1.32 \times 10^{-1} \pm 0i$	$-9.69 \times 10^{-1} \mp 2.11 \times 10^{-1} i$
2	0.2	$-1.03 \times 10^{-5} \pm 1.42 \times 10^{-2} i$	$9.79 \times 10^{-1} \pm 0i$	$1.18 \times 10^{-1} \pm 1.69 \times 10^{-1} i$
		$-6.42 \times 10^{-7} \pm 2.03 \times 10^{-3} i$	$1.31 \times 10^{-1} \pm 0i$	$-9.73 \times 10^{-1} \mp 1.91 \times 10^{-1} i$
4	1.5	$-1.08 \times 10^{-4} \pm 1.41 \times 10^{-2} i$	$9.70 \times 10^{-1} \pm 0i$	$1.70 \times 10^{-1} \pm 1.75 \times 10^{-1} i$
		$8.61 \times 10^{-5} \pm 2.78 \times 10^{-3} i$	$2.63 \times 10^{-1} \pm 0i$	$-9.55 \times 10^{-1} \mp 1.35 \times 10^{-1} i$

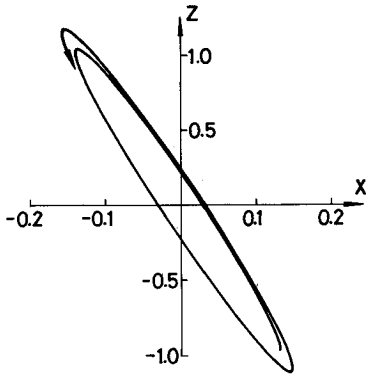

Fig. 2 Example of motion of subsatellite.

it can be seen from Eqs. (15) and (16) and the Routh-Hurwitz stability criterion that the system is stable if, and only if,

$$\lambda < 3\{1 - Z_s^2/(2l_0^2)\}/\{R\epsilon(1 - \Omega/\omega)\} \tag{21}$$

where

$$\epsilon \equiv (l_s - l_0)/l_0 \ll 1 \tag{22}$$

$$l_0/R \ll 1 \tag{23}$$

have been assumed and they have been neglected compared with unity. This fact means that the motion is unstable if the atmospheric density gradient is greater than a certain value. Since

$$\epsilon = 3m\omega^2 l_s/EA \tag{24}$$

$$Z_s = -\rho_s C_D S R^2 (1 - \Omega/\omega)^2/(6m) \tag{25}$$

can be derived from Eqs. (10–13), it can be seen that the right-hand side of inequality (21) decreases, i.e., the unstable region expands, as the value of EA/m decreases and/or the value of $\rho_s C_D S/m$ increases.

Numerical Example

As an example, the case of

$$R = 6.6 \times 10^6 \text{ m}, \quad \omega = 1.18 \times 10^{-3} \text{ s}^{-1}, \quad EA/m = 20 \text{ N/kg}$$

$$l_0 = 10^5 \text{ m}, \quad \Omega = 7 \times 10^{-5} \text{ s}^{-1}, \quad \rho_s C_D S/m = 2 \times 10^{-9} \text{ m}^{-1}$$

is investigated. The example roughly corresponds to a subsatellite deployed to the altitude of 115 km with the projected drag area, S, of 10 m^2 (which is a sum of the 2 m^2 projected area of the subsatellite and the effective area of 8 m^2 of the lowest portion of the 1.2-mm-diam tether), mass of 500 kg, and the drag coefficient of 2.2. The steady-state solutions can be obtained from Eqs. (10–13) as

$$X_s = -1.01 \times 10^5 \text{ m}, \quad Z_s = -1.28 \times 10^4 \text{ m}$$

$$T_s = 4.27 \times 10^2 \text{ N}, \quad l_s = 1.021 \times 10^5 \text{ m}$$

From these values, the right-hand side of inequality (21) can be obtained as 2.25×10^{-5} m^{-1}. The eigenvalues and eigenvectors in the cases of $\lambda = 1.5 \times 10^{-4}$ m^{-1} and $\lambda = 2.0 \times 10^{-5}$ m^{-1} are shown in Table 1. It can be seen that the system is unstable in the former case and stable in the latter, as can be expected from inequality (21). Figure 2 shows an example of motion of unstable mode, which can be obtained from the eigenvector. It can be seen that the locus of motion is like a growing slender ellipse. The eigenvalues and eigenvectors of the case of $\rho_s C_D S/m = 4 \times 10^{-9}$ m^{-1}, which roughly corresponds to the altitude of 110 km, is also listed in Table 1. A more rapid divergence of swinging can be seen from the eigenvalues in the case of greater value of $\rho_s C_D S/m$.

Interpretation of the Phenomena

The phenomena of instability can be interpreted as follows: When the subsatellite moves around the steady-state equilibrium point, the angular velocity of the subsatellite around the main satellite is $\omega + \dot{\theta}$. Therefore, when the value of $\dot{\theta}$ is positive, the centrifugal force increases, the tether elongates, as can be seen in Fig. 2, the altitude of the subsatellite decreases, the atmospheric density around the subsatellite increases, and the aerodynamic drag increases. When the value of $\dot{\theta}$ is negative, the aerodynamic drag decreases. It is clear that this difference in the drag force is in the direction to excite the swinging vibration.

Conclusions

An atmospheric density gradient greater than a certain value causes instability in the in-plane swinging motion of uncontrolled tethered subsatellite deployed in a low-altitude Earth orbit. The unstable region expands as the longitudinal rigidity of the tether decreases and/or the atmospheric drag increases. It seems important to investigate the effect of the atmospheric density gradient on the control system design as a future work. (After the final revision, the authors found that the instability investigated in this Note also had been briefly mentioned in Ref. 3.)

References

[1]Bainum, P. M., Diarra, C. M., and Kumar, V. K., "Shuttle-Tethered Subsatellite System Stability with a Flexible Massive Tether," *Journal of Guidance, Control, and Dynamics*, Vol. 8, Jan.–Feb. 1985, pp. 230–234.

[2]Yuhara, N., Sato, C., and Kawakami, M., "On Lumped Model of Tethered Satellites," *Proceedings of the 30th Space Science and Technology Conference*, Sept. 1986, pp. 530–531 (in Japanese).

[3]Beletskii, V. V. and Levin, E. M., "Dynamics of the Orbital Cable System," *Acta Astronautica*, Vol. 12, May 1985, pp. 285–291.